

1 **TITLE**

2 Intercomparison of MODIS albedo retrievals and in situ measurements across the global FLUXNET
3 network.

4

5 | Author list

6 Alessandro Cescatti^a, Barbara Marcolla^b, Suresh K. Santhana Vannan^c, Jerry Yun Pan^c, Miguel O.
7 Román^d, Xiaoyuan Yang^e, Philippe Ciais^f, Robert B. Cook^c, Beverly E. Law^g, Giorgio Matteucci^h,
8 Mirco Migliavacca^a, Eddy Moorsⁱ, Andrew D. Richardson^j, Günther Seufert^a, Crystal B. Schaaf^e

9

10

11

12 Affiliations

13 *a* European Commission - DG Joint Research Centre, Institute for Environment and Sustainability,
14 Climate Change Unit, Ispra 21027 Italy

15 *b* Edmund Mach Foundation, IASMA Research and Innovation Centre, 38010 S. Michele all'Adige
16 38010, Italy

17 *c* Environmental Sciences Division, Oak Ridge National Laboratory, Oak Ridge, TN 37831 USA

18 *d* Hydrospheric and Biospheric Sciences Laboratory, NASA Goddard Space Flight Center, Greenbelt,
19 MD, United States

20 *e* Center for Remote Sensing, Department of Geography and Environment, Boston University, 725
21 Commonwealth Avenue, Boston MA 02215 USA

22 *f* Laboratoire des Sciences du Climat et de l'Environnement (LSCE), Joint Unit of CEA-CNRS-UVSQ,
23 Gif-sur-Yvette, France

24 *g* Department of Forest Ecosystems & Society, Oregon State University, Corvallis, OR, USA

1 *h* CNR-ISAFOM, Via Cavour, 4-6, 87036 Rende, CS, Italy

2 *i* ESS-CC, Alterra Wageningen UR, Wageningen, Netherlands

3 *j* Harvard University, Department of Organismic and Evolutionary Biology, Harvard University

4 Herbaria, 22 Divinity Avenue, Cambridge MA 02138 USA

5

6

7 Corresponding author

8 Alessandro Cescatti alessandro.cescatti@jrc.ec.europa.eu

9 European Commission - DG Joint Research Centre

10 Institute for Environment and Sustainability

11 Climate Change and Air Quality Unit, TP290

12 Via E. Fermi, 2749, I-21027 Ispra (VA), ITALY

13 Tel: +39 0332 78 5582

14 Fax: +39 0332 78 5704

15

1 **Abstract**

2 Surface albedo is a key parameter in the Earth's energy balance since it affects the amount of solar
3 radiation directly absorbed at the planet surface. Its variability in time and space can be globally
4 retrieved through the use of remote sensing products. To evaluate and improve the quality of satellite
5 retrievals, careful intercomparisons with in situ measurements of surface albedo are crucial. For this
6 purpose we compared MODIS albedo retrievals with surface measurements taken at 53 FLUXNET
7 sites that met strict conditions of land cover homogeneity. A good agreement between mean yearly
8 values of satellite retrievals and in situ measurements was found ($R^2= 0.82$). The mismatch is
9 correlated to the spatial heterogeneity of surface albedo, stressing the relevance of land cover
10 homogeneity when comparing point to pixel data. When the seasonal patterns of MODIS albedo is
11 considered for different plant functional types, the match with surface observation is extremely good at
12 all forest sites. On the contrary, in non-forest sites satellite retrievals underestimate *in situ*
13 measurements across the seasonal cycle. The mismatch observed at grasslands and croplands sites is
14 likely due to the extreme fragmentation of these landscapes , as confirmed by geostatistical attributes
15 derived from high resolution scenes.

16 **Keyword:** MODIS, surface albedo, validation, FLUXNET, terrestrial ecosystems, plant functional
17 types, remote sensing,

18 **1. Introduction**

19 Land surface broadband albedo directly affects Earth's climate by determining the fraction of
20 shortwave radiation absorbed at the ground and therefore influencing the surface energy budget
21 (Dickinson, 1983). Surface albedo is a crucial parameter in determining the magnitude of energy fluxes
22 in the soil–plant–atmosphere continuum (Bonan, 2008; Chapin et al., 2008), affecting surface
23 temperature, evaporation and transpiration, cloud formation and precipitation, thus ultimately
24 impacting gross primary productivity (Dickinson, 1983; Lawrence & Slingo, 2004; Ollinger et al.,

1 2008; Sellers et al., 1997). Several authors have investigated the interplay between albedo and drought
2 (Govaerts & Lattanzio, 2008) or fires (Randerson et al., 2006), and the climate sensitivity to variation
3 in surface albedo caused by major changes in land cover as the expansion of agricultural land in the
4 northern hemisphere during the 18th century (Myhre et al., 2005; Vavrus et al., 2008). Surface albedo is
5 also a key factor in the expected positive feedback between surface temperature and global warming at
6 northern latitudes (Chapin et al., 2005) and may play a relevant role in offsetting the carbon
7 sequestration potential of afforestation programs (Anderson et al., 2010; Betts, 2000; Betts et al., 2007;
8 Bird et al., 2008; Rotenberg & Yakir, 2010).

9 Given the relevance of surface albedo in the Earth's climate system, monitoring this parameter in space
10 and time is fundamental for the development of global climate models (Alton, 2009; Frida A-M et al.,
11 2006; Hollinger et al., 2009; Tian et al., 2004) and for climate change and ecosystem research in
12 general (Betts, 2000; Charlson et al., 2007; Charney et al., 1977; Dirmeyer & Shukla, 1994; Hall & Qu,
13 2006; Henderson-Sellers & Wilson, 1983; Pinty et al., 2011a). An important step toward the
14 availability of global surface spectral albedo has been the launch of NASA's Terra and Aqua satellites
15 and the MODerate-resolution Imaging Spectroradiometer (MODIS) (Lucht et al., 2000b; Salomonson
16 et al., 1989; Schaaf et al., 2002). The MODIS sensor provides global maps of surface albedo
17 reconstructed from retrieved models of reflectance anisotropy at a 500-m gridded spatial resolution
18 every 16 days for the first seven MODIS spectral bands (0.47–2.1 μm) and for three broadband regions
19 (0.3–0.7, 0.7–5.0, and 0.3–5.0, μm) (Lucht et al., 2000b; Moody et al., 2008; Schaaf et al., 2002).

20 Comparing satellite albedo retrievals with surface measurements and with independent satellite
21 products is fundamental in evaluating the accuracy of remote sensing products and improving retrieval
22 algorithms (Liang et al., 2002; Pinty et al., 2011b). Several recent studies have evaluated the
23 consistency of global albedo products using in situ data at various spatial and temporal scales (Chen et
24 al., 2008; Jin et al., 2003a; Jin et al., 2003b; Liang et al., 2002; Liu et al., 2009; Román et al., 2010;
25 Román et al., 2009; Wang et al., 2010) and under specific snow cover conditions (Stroeve et al., 2005).

1 Most of these studies stress that a direct comparison is very challenging because of scale mismatch and
2 heterogeneity of the land surface at the satellite measurement scale that reduces the spatial
3 representativeness of ground point measurements (Liang et al., 2002; Román et al., 2010; Román et al.,
4 2009). As a consequence, a careful selection of ground points and the characterisation of their spatial
5 representativeness are crucial for a meaningful point-to-pixel comparison (Liang et al., 2002; Lucht et
6 al., 2000a; Román et al., 2009).

7 Intercomparisons of surface and satellite albedo have been performed so far at a limited number of
8 locations (Jin et al., 2003a; Liu et al., 2009; Román et al., 2010; Román et al., 2009; Salomon et al.,
9 2006; Wang et al., 2010) and a global analysis across different continents and plant functional types
10 (PFTs) is still lacking. The objective of this work is to provide a comprehensive intercomparison in
11 time and space of in situ measurements and satellite retrievals of snow-free broadband surface albedo.
12 For this purpose we compared MODIS gridded albedo retrievals at the 500-m scale with ground
13 measurements performed across the FLUXNET network (Baldocchi et al., 2001), the largest global
14 data set of energy and mass flux measurements at ecosystem scale.

15 The geographical extent of the terrestrial data set allowed the comparison of several PFTs in a
16 comprehensive and consistent way across the seasonal cycle. In addition, the large number of
17 experimental sites in the network provided an unprecedented opportunity to perform a careful
18 evaluation of the surface heterogeneity at the reference plots, based on a combination of qualitative and
19 quantitative metrics. For this purpose images from Google Earth, MODIS and Enhanced Thematic
20 Mapper Plus (ETM+) have been used at various spatial scales (from 1x1 to 7x7 km). Differences
21 between satellite retrievals and in-situ albedo have been analyzed as a function of surface
22 heterogeneity, PFT and seasonality. Results of the intercomparison have been finally discussed
23 considering the different sources of uncertainty that affect the terrestrial and satellite datasets.

24

25

1 **2. Materials and methods**

2 **2.1. Surface data set**

3 In this study, we used in situ radiometric measurements available in the FLUXNET “La Thuile”
4 database (www.fluxdata.org, October 2010) released in December 2007, which includes half hourly
5 observations of ecosystem fluxes and meteorological data from more than 250 sites, for a total of 960
6 site-years.

7 Albedo is computed as the ratio of downward and upward global radiation as observed with double
8 pyranometers (e.g. CMA-11, CMA-6 or CNR-1, Kipp&Zonen, Delft, The Netherlands). Surface albedo
9 is typically estimated in the spectral range 280-2800 nm (accounting for more than 98.5% of the
10 surface solar radiation according to ASTM G-173 reference spectra) and is therefore comparable with
11 the broadband MODIS albedo (300-5000nm). Giving that the field of view (FOV) of pyranometers is
12 typically 180 deg, the footprint of surface reflectance measurements is theoretical infinite. However,
13 due to the cosine response of the sensor, 50% of the signal originates in a FOV of 90 deg and 80% in a
14 FOV of 127 deg. The footprint of surface albedo therefore depends on the height of the albedometer
15 above the canopy top (ranging from 5 to 10 m) and typically extends up to 10-20 m from the tower at
16 80% of the signal.

17 The uncertainty of surface albedo measurements depends on the absolute accuracy of pyranometers
18 (about 5%) and on the non-ideal cosine response (about 3%). Most of the errors associated with the
19 absolute accuracy of the instrument are similar for upward and downward fluxes and therefore
20 compensate. Overall the expected accuracy is in the order of 4-7% in clear sky and 1-4% in overcast
21 condition (Pirazzini, 2004; Pirazzini et al., 2006).

22 The geographical distribution of the sites is strongly clustered in Europe and North America (97 and
23 106 sites corresponding to 38% and 42% of the total), which are the regions with the longest history of
24 continuous ecosystem flux measurements (Baldocchi et al., 2001). Several sites in the database are

1 located in tropical Amazonia and East Asia, while the coverage in Africa, Central Asia, and Australia
2 remains sparse and limited in the number of observation years. Despite the uneven geographical
3 distribution, the “La Thuile” database guarantees a good coverage of the most important plant
4 functional types, among which evergreen needle leaf forest (ENF), grassland (GRA), deciduous
5 broadleaf forest (DBF), and cropland (CRO) are the most represented with respectively 28%, 18%,
6 13% and 12% of the sites.

7 Out of the 138 FLUXNET sites reporting continuous measurements of incoming and outgoing
8 shortwave radiation (300-2800 nm; CMA-11, CMA-6 or CNR-1, Kipp&Zonen, Delft, The
9 Netherlands) 18 have been excluded after a QA/QC analysis of the albedo data series. The QA/QC
10 procedure was based on the following criteria: occurrence of an offset in the incoming or reflected
11 radiation (night-time data systematically and significantly different from zero), occurrence of phase lag
12 between incident and reflected radiation and systematic occurrence of unrealistic values (e.g. reflected
13 radiation higher than incident radiation).

14 The land cover characteristics of the remaining 120 sites have been carefully classified using high
15 resolution satellite images (available via Google Earth™), to identify those matching the requirement
16 of homogeneity in the area surrounding the measurement tower (Jin et al., 2003b; Román et al., 2010;
17 Román et al., 2009). Although MODIS albedo is gridded at 500-m resolution the land classification has
18 been performed at 1km², taking into account the uncertainty in the geospatial registration of satellite
19 products and the fact that the albedo retrieval algorithm is based on multi-angle observations covering
20 larger areas at edge of scan.

21 The classification process was based on the following four steps:

- 22 1. visual identification of the number and extension of different PFTs in the 1km² area
23 surrounding the tower;
- 24 2. verification of the correspondence between the dominant PFT in the 1km² area and the PFT at
25 the tower site as reported in the FLUXNET database;

- 1 3. qualitative ranking of landscape heterogeneity in three classes (low, medium, high) based on the
- 2 plant canopy characteristics (tree density, patchiness, etc.);
- 3 4. attribution of a confidence level in the classification of the sites (low, medium, high) based on
- 4 the quality of the image.

5 To guarantee the highest level of homogeneity and to minimize issues associated with spatial
6 representativeness in the point-to-pixel comparison, only those sites characterized by the lowest level
7 of heterogeneity and with only one PFT in the 1km² area were included in the analysis.

8 **2.2. MODIS products**

9 The MODIS albedo retrievals at the FLUXNET sites were generated using three MODIS products,
10 namely, MCD43A1 (BRDF-Albedo Model Parameters 16-Day L3 Global 500m), M*D04 (Aerosol
11 product daily L2 Global 10km), and MCD43A2 (BRDF-Albedo Quality 16-Day L3 Global 500m). All
12 these products are from the Collection V005 MODIS reprocessing campaign. The MODIS surface
13 reflectance anisotropy and albedo product is based on all high quality, cloud-free, atmospherically
14 corrected surface reflectances that are obtained over a 16-day period. When sufficient observations are
15 available to adequately sample the surface anisotropy, an appropriate rendition of the
16 RossThickLiSparseReciprocal Bidirectional Distribution Reflectance Model (BRDF) model is retrieved
17 (Lucht et al., 2000b; Schaaf et al., 2002). This retrieval is attempted every 8 days at a 500 m gridded
18 resolution. This retrieval model is used to generate intrinsic values of clear-sky direct surface albedo
19 (referred to as directional hemispherical reflectance or black-sky albedo) and wholly diffuse albedo
20 under isotropic illumination (bihemispherical albedo or white-sky albedo). These can be combined
21 under particular illumination and atmospheric aerosol optical depth conditions (Lucht et al., 2000b;
22 Román et al., 2010) to provide clear-sky albedos comparable to those measured *in situ* at a flux tower.
23 Albedo quantities are reported at a 500-m gridded resolution, but all multi-angle observations that
24 encompass areas are utilized in the retrieval. Therefore, although extended observation coverage is

1 somewhat compensated for in the retrieval process, it is best to consider regions larger than 500 m
2 when comparing observations made from satellite to those made on the ground.

3 The calculation of clear-sky surface albedo at the tower sites involved the following two steps. The first
4 step was the generation of the aerosol optical depth values for each site and each calendar date using
5 the MODIS – Terra (MOD04) and MODIS-Aqua (MYD04) aerosol swath products. To generate the
6 optical depth, the MODIS Adaptive Processing System - MODAPS (Masuoka et al., 2000; Masuoka et
7 al., 2007) was used to prepare M*04 subsets at 50 x 50 km region centered at the site. All pixels that
8 had optical depth values greater than 0.35 or a cloud fraction greater than 0.6 were filtered out and not
9 used in the optical depth generation. All pixels that had fill values for solar zenith angle were also
10 rejected. After the filters were applied, a combined M[OY]D optical depth file was generated for each
11 site, taking valid optical depth values from Terra and Aqua and generating one mean value for the
12 optical depth per site per day. This method of course is not as accurate as having instantaneous sun
13 photometer data (Holben et al., 1998) at the site, but the mean gives an approximation of the aerosol
14 optical depth over the local solar noon.

15 The second step was the calculation of the clear sky surface albedo on the basis of the MODIS-derived
16 550nm aerosol optical depths calculated in the previous step, the local solar zenith angle, the
17 MCD43A1 product, and QA flags from MCD43A2 for each site involved in the analysis and for each
18 date. If a date has no valid MCD43A1 pixels or if the optical depth was a fill value, no albedo was
19 calculated for that date. As far as quality criteria are concerned only “full BRDF inversion” pixels
20 (QA=0 processed, good quality) were included in the calculation, while the "Snow_BRDF_Albedo"
21 band of the MCD43A2 product was used to identify and exclude snow albedo retrievals. Following this
22 procedure clear-sky MODIS albedo at local solar noon were retrieved at each FLUXNET site for all
23 days with available aerosol MODIS product (M*D04) information, snow-free conditions, and solar
24 elevation angles greater than 20 deg. On the same dates, the flux tower measurements of albedo have
25 been averaged for the hour centered at solar noon.

1 To integrate the observations at the FLUXNET sites in the global picture, snow-free global albedo
2 averages per PFT and latitudinal band were computed from the MODIS V005 0.05 degree Climate
3 Modeling Grid (CMG) product and stratified with the MCD12C1 land cover product. Yearly averages
4 have been calculated on each pixel fulfilling the following requirements: QA=0 (majority processed,
5 good quality), snow coverage less than 10% (based on MODIS estimates), and major PFT coverage
6 greater than 70% of the pixel. Note that the 0.05 degree MCD43C1 product is an average of the 500m
7 pixel underlying each 0.05 degree pixel and the quality flag only represents the quality of the majority
8 of the underlying pixels.

9 **2.3. Landscape heterogeneity**

10 One of the key issues in the intercomparison of satellite retrieval and surface observations is the
11 objective and quantitative evaluation of landscape heterogeneity and the representativeness of in situ
12 measurements (Liang et al., 2002; Román et al., 2009; Susaki et al., 2007).

13 For this purpose we applied the methodology presented by Román et al. (2009) and based on the
14 estimation of geostatistical attributes from high resolution scenes (Enhanced Thematic Mapper Plus).
15 The spatial patterns and scales of landscape heterogeneity have been estimated from variogram models
16 fitted at FLUXNET sites over the spatial scales of MODIS observations.

17 In synthesis, the methodology adopted for the estimation of geostatistical indexes is based on the
18 comparison of variogram model parameters retrieved at different spatial resolution (i.e. from 1.0 km² to
19 1.5 km² squared subsets). By examining the variogram parameters at two scales, the spatial
20 characteristics of a given measurement site is compared against the larger landscapes extending to
21 several MODIS pixels.

22 Four different geostatistical attributes of spatial representativeness have been used to describe the
23 overall variability (R_{CV}), spatial extent (R_{SE}), strength of the spatial correlation (R_{ST}), and

1 spatial structure (R_{ST}) of surface albedo for a given measurement site. Further details on the methods
2 and algorithms used to calculate these attributes are reported in Román et al. (2009).
3 Using a weighted combination of the four geostatistical attributes a comprehensive metric of the
4 landscape heterogeneity (ST_{score}) has been computed to evaluate and compare FLUXNET sites:

$$ST_{score} = \frac{|R_{ST}| + |R_{SD}| + |R_{SD}|}{3} -$$

5 In addition, the landscape heterogeneity at a larger spatial scale (7x7 km) has been quantified as the
6 standard deviation of MODIS albedo (14 x 14, 196 pixels) area centered at the FLUXNET site.

7

8

9

10

1 **3. Results and discussion**

2 **3.1. The terrestrial data set: spatio-temporal distribution and representativeness**

3 As a result of the visual classification of land cover characteristics, 49% of the 120 sites performing
4 reliable continuous measurements of broadband albedo were rejected for reasons of landscape
5 heterogeneity and 7% because of low confidence in the PFT classification.

6 Of the remaining 53 sites (among which there were 15 ENF, 8 CRO, 7 DBF, and 7 evergreen broad-
7 leaf forests (EBF)) the largest fraction is located in Europe (19) and North America (15 USA, 7
8 Canada). The remainder of the sites are located in Africa (4), South America (3), Asia (3) and Australia
9 (2) (Fig. 1, Table 1).

10 **[Figure 1]**

11 **[Table 1]**

12 Across all sites, 18666 days of synchronous MODIS retrievals and in situ surface albedo were
13 available. On average, this worked out to 333 and 400 days of data for each forested and non-forested
14 site, respectively (on average about 80 observations per site and year), but there was considerable
15 variability among sites. To date, this is the largest data set that has been used to compare satellite and in
16 situ albedo measurements.

17 Although the data set spans the years 2000-2007, the vast majority (87%) of observations were made
18 between 2003 and 2006 (Fig. 2a). Because of filtering for snow and cloud cover, and the dominance of
19 Northern hemisphere sites in the data set, the number of observations is lower during winter months
20 (November through February) (Fig. 2b).

21 **[Figure 2]**

22 The seasonal variation of the global average of snow-free albedo is remarkably small for forests, likely
23 because ~70% of the sites are evergreen forests with leaf area index, canopy structure and chemistry
24 not as dynamic as those of deciduous ecosystems. The seasonal trend of snow-free albedo is somewhat

1 more pronounced for non-forest ecosystems, which include crops and grasslands (Running et al., 1995)
2 (Fig. 2b).

3 The spatial representativeness of the FLUXNET albedo data set in the global albedo domain has been
4 explored by superimposing the MODIS retrievals at the sites on the global distribution of MODIS
5 albedo (Fig. 3) for the same PFT or latitudinal class. Concerning the latitudinal distribution, 75% of
6 FLUXNET sites are clustered in the 30-55° N band (Fig. 3a), and in this latitude band the surface
7 albedo observed at the sites is substantially lower (20%) than the MODIS latitudinal average. This is
8 due to the non-representative distribution of FLUXNET sites, which are mostly located in dense and
9 productive temperate forests of the Northern Hemisphere. The difference between latitudinal MODIS
10 averages and site-measurements of albedo is less evident in the Southern hemisphere, where also the
11 number of FLUXNET site is remarkably lower.

12 **[Figure 3]**

13 In terms of PFTs (Fig 3b), 79% of sites analyzed here are classified as one of ENF, EBF, CRO, GRA or
14 DBF. When PFT averages are compared with the global average of MODIS albedo, most of the sites
15 fall within the 10-90 percentile intervals of the global MODIS observations, with the exception of EBF
16 for which MODIS retrievals at the sites show lower values of albedo. For the other PFTs (woody
17 savanna (WSA), open shrubland (OSH), savanna (SAV), mixed forest (MF)) the number of sites is too
18 low to speculate on the global representativeness of the FLUXNET dataset.

19

20 **3.2. Point to pixel comparison**

21 The comparison of MODIS albedo retrievals with in situ measurements has been limited to the
22 FLUXNET sites with the highest degree of homogeneity in order to minimize the effect of the scale
23 mismatch. Examples of high resolution images (available via Google Earth™) used to evaluate site
24 homogeneity are reported in Fig. 4 for four test sites.

1 **[Figure 4]**

2 The time series of MODIS retrievals and in situ measurements at these four sites show contrasting
3 results (Fig. 5). At some sites the match is extremely good both in terms of absolute values and
4 seasonal trend (e.g. US-MMS, US-FPe). At other locations MODIS retrievals show a systematic
5 overestimation (e.g. PT-Esp) or underestimation (e.g. ES-LMa) of surface measurements. These biases
6 are probably due to the fine-scale spatial variability of the plant cover and to the representativeness of
7 the tower footprint in the MODIS pixel, since the other sources of uncertainties (sensor calibration,
8 uncertainty of AOD estimates, etc.) cannot explain such large and systematic errors. In particular at
9 sites with discontinuous plant canopies like ES-LMa (Fig. 4), the height from the ground and the spatial
10 location of the albedometer are critical factors, determining the representativeness of the in situ
11 measurements at the resolution of the satellite pixel.

12 **[Figure 5]**

13 A good agreement between satellite and in situ measurements was found when sites were grouped
14 according to PFT (Fig. 6a, type II regression, $R^2= 0.82$). Forest PFTs (such as ENF, EBF, MF) fall in
15 the lower part of the graph, while non-forest PFTs (such as CRO, GRA, wetlands (WET)) in the upper
16 part. Albedo is correlated to several plant-level traits including leaf albedo, leaf area index, vertical
17 angle of leaves/needles, the degree of foliage and canopy clumping, and the geometric-optical
18 shadowing due to canopy structure. It is well known that the structural canopy traits typical of tall
19 canopies trap more of the incoming radiation, therefore reducing the canopy albedo of forest PFTs
20 (Cescatti, 1998; Davidson & Wang, 2004).

21 **[Figure 6]**

22 Satellite retrievals and surface measurements at the site level (Fig. 6b) show a coefficient of
23 determination of 0.83, very similar to that observed in the comparison by PFT and reported in
24 comparable studies (Wang et al. 2010). Both regressions in Fig. 6 show a slope lower than one (0.88
25 and 0.74 for panel (a) and (b), respectively), primarily due to the different spatial scale of the two

1 estimates, with the satellite retrievals referring to a considerably larger area than tower measurements.
2 The spatial averaging of surface albedo on the large MODIS pixels dampen the variability when
3 compared with high-resolution imagery or point measurements and ultimately determines the trend
4 (intercept >0 and slope <1) of the regressions in Fig. 6. Similar slope and closer correlations have been
5 observed by comparing early MODIS retrievals with surface measurements using high-resolution
6 remotely sensed imagery (Landsat7 ETM+) to characterize the land cover heterogeneity in the MODIS
7 pixel (Liang et al., 2002). The negative bias of MODIS at the sites with larger albedo has been reported
8 also by Wang et al. (2010) and has been mostly attributed to the underestimation of visible albedo.
9 The mean error and mean absolute error of the MODIS retrievals vs. the in situ observations are
10 reported in Fig. 7a together with the R^2 of the regression computed for the single sites. The mean error
11 is a measure of the retrieval accuracy and is on average negative (-0.004) implying that the magnitude
12 of the MODIS surface albedo is on average slightly lower than in situ observations. It is also interesting
13 to notice that the spread is considerably larger among the sites with a negative error both in terms of
14 mean error and mean absolute error. The R^2 observed at single sites, proportional to dot size in Fig. 7a,
15 is largely independent of the mean error since it mostly depends on the seasonal variability of the
16 measurements. For this reason, sites with a marked seasonality in albedo (i.e. deciduous forests, crops
17 and boreal ecosystems) typically show a higher R^2 than tropical or Mediterranean evergreen forests.
18 The error distribution peaks in the -0.01 class and is skewed to the left, with larger errors at sites where
19 MODIS underestimates surface measurements (Fig. 7b). The mean values of STscore (geostatistical
20 index proportional to the representativity of in-situ measurements in the MODIS pixel) in the different
21 classes of mean error shows several interesting features (Fig. 7b). The highest mean value of the score
22 (3.9) is in the class at zero mean error, confirming the validity of this approach to quantify the spatial
23 representativeness of experimental sites. The values of ST_{score} is considerably lower (1-1.4) at sites
24 characterized by a negative error (MODIS $<$ in situ) and the variability of this index is rather limited
25 between sites. At these sites the towers are probably located in a brighter spot than the average of the

1 pixel and typically pertain to the categories of grassland (GRA) or cropland (CRO) (Table 2). On the
2 contrary sites with a positive bias (MODIS>In situ albedo), where the tower spot is located on an area
3 darker than the surroundings, show intermediate value of the score (2.5) and a large variability between
4 sites.

5 **[Figure 7]**

6 **[Table 2]**

7 Giving that the MODIS albedo product is reported at 500 m resolution while the retrieval algorithm is
8 based on multiangular reflectances that extend over this area, landscape heterogeneity at scales larger
9 than 500 m may ultimately affect the uncertainty in the retrievals. To assess the impact of the spatial
10 heterogeneity on the accuracy of MODIS retrievals we computed the mean absolute percentage error
11 for sites ensembles at increasing levels of spatial variability (expressed as standard deviation of
12 MODIS albedo in the $7 \times 7 \text{ km}^2$ area surrounding the site or as ST_{score}). Figure 8 shows that the error
13 between satellite and in situ measurements increases with the spatial variability of albedo, further
14 demonstrating the crucial issue of the spatial variability of surface albedo in the point to pixel
15 intercomparisons.

16 Both MODIS standard deviation and ST_{score} show sharp variations for values of the mean absolute
17 percentage error up to 12%. Above this threshold both indexes are no longer correlated with the error.
18 The trend of the two spatial indexes is remarkably similar though in opposition, since MODIS standard
19 deviation increases with the spatial variability while ST_{score} increases with spatial homogeneity. Despite
20 the different spatial domain (7×7 and 1.5 km) the two indexes are strongly correlated (Fig. 8 inset) with
21 an R^2 of 0.90. These results demonstrate that a close match between surface measurements and satellite
22 retrievals is achievable only at the most spatially homogenous sites, where the canopy optical
23 properties are scale-invariant. These golden sites can be effectively detected with both statistical
24 analysis of MODIS albedo or with higher resolution images and detailed geostatistical indexes.

1

2 **[Figure 8]**

3 **3.3. Seasonal trends**

4 Seasonal patterns in the relationship between site-level averages of MODIS and FLUXNET albedo are
5 reported in Figure 9. In all seasons, the relationship between MODIS (y axis) and in situ (x axis) albedo
6 has a slope ranging from 0.71 to 0.74 and positive intercept, meaning that MODIS over-estimates
7 surface albedo of low-albedo sites, and under-estimates albedo of high-albedo sites. The lowest
8 correlation ($R^2=0.73$) is observed for winter values (from December to February) and the highest
9 ($R^2=0.82$) for fall values (from September to November). Similarly, larger differences between in situ
10 and satellite based estimation of surface albedo in winter season were observed in Jin et al. (2003), who
11 suggested that this was the result of the increased heterogeneity of surface reflectivity due to the
12 presence of residual snow and canopy heterogeneity.

13 **[Figure 9]**

14 The inset in Fig. 9a shows the correlation matrix of the errors observed in the different seasons. All
15 correlation coefficients are positive, meaning that sites with surface measurements larger than satellite
16 retrievals in one season tend to have the same behaviour in the other seasons. Thus, site-specific biases
17 are coherent over time, possibly indicating mismatches between the footprint of tower radiometric
18 instruments and the corresponding MODIS pixel, calibration errors of the tower radiometric
19 instruments, inappropriate estimation of aerosol optical depths or systematic errors in MODIS retrieval.

20 **[Figure 10]**

21 In Figure 10 the seasonal trends of satellite and in situ data for a set of PFTs are reported with their
22 standard deviation, and superimposed on the range of MODIS albedo observed at the global scale for
23 the same PFTs (grey bands represent the 10-90 percentile interval). An exceptionally good agreement
24 between the two independent albedo estimates is observed for forest PFTs, both in terms of absolute

1 albedo values and seasonal patterns. In contrast, for non-forest PFTs (CRO and GRA) MODIS
2 retrievals are systematically smaller than surface measurements, while their respective seasonal
3 patterns are in agreement as observed also by Davidson & Wang (2004). The mismatch observed at the
4 non-forest sites is likely due to the extreme fragmentation of these landscapes and to the very limited
5 spatial footprint of surface radiometric measurements performed at these sites (i.e. over short
6 vegetation albedometers are typically installed few meters above ground). Wang et al. (2010) reported
7 that the average negative bias of MODIS albedo is probably due to the underestimation of visible
8 surface reflectance and that this phenomenon may be more pronounced for herbaceous canopies with
9 larger albedo in the visible bands.

10 The large variability of CRO and GRA surface albedo (Fig. 10) can be ascribed to the spatial variability
11 in LAI, to the variable amount of exposed soil and soil moisture content, to the rapid temporal dynamic
12 of the canopy in response to climatic drivers like temperature and water status (Gao et al., 2005) as well
13 as to management practices (e.g. planting, harvesting, grazing, crop type, etc.) (Tittebrand et al., 2009).
14 Given the large spatial variability of GRA and CRO albedo, future intercomparison of satellite and in
15 situ observation for these PFTs should be performed preferentially at selected sites with homogenous
16 crop cover and management practices at the MODIS spatial resolution.

17 ENF and EBF snow-free albedo do not show any significant seasonal trend and monthly values are
18 around 0.1. EBF do not show seasonal variation also at the global scale, while larger variability is
19 observed for ENF in winter months. A clear seasonality is shown by DBF+MF and CRO, with higher
20 values at the peak of the growing season, in line with the results of other in situ studies (Sellers et al.,
21 1997). The seasonal pattern of GRA is the opposite, with a winter maximum in albedo. The increase of
22 GRA albedo from August, observed both in MODIS and FLUXNET data, is probably due to vegetation
23 senescence, with the increase of exposed soil and dead biomass and the drying of stalks and seeds
24 during summer months.

25

1 **4. Conclusions**

2 Surface albedo is a key parameter in the Earth's energy balance since it affects the amount of solar
3 radiation directly absorbed at the planet surface. Its variability in time and space can be retrieved
4 through the use of remote sensing products, available nowadays at high temporal and spatial resolution
5 from different satellite platforms (e.g. Terra and Aqua MODIS observations are used to retrieve albedo
6 every 16 days at a spatial resolution of 500 x 500 m starting March 2000).

7 Careful intercomparisons with in situ measurements of surface albedo are crucial to evaluate and
8 improve the quality of remote sensing products. In this context the "La Thuile" FLUXNET dataset
9 offers an unprecedented opportunity to select sites according to strict conditions of landscape
10 homogeneity and across a wide range of PFTs and geographical areas. When compared to the
11 latitudinal distribution of surface albedo, the FLUXNET data set clearly shows a bias towards darker
12 vegetated areas in the Northern hemisphere. In this respect, the biased distribution of the terrestrial
13 dataset in the global albedo domain should be taken into account when using in situ FLUXNET albedo
14 data in the parameterization of land surface models.

15 The key issue in the intercomparison of satellite and in situ measurements is the spatial
16 representativeness of the latter in the satellite pixel. The MODIS pixel can be 100-1000 times larger
17 than the footprint of in situ observations, depending on the height of the albedometer above the canopy
18 top. For this reason a careful classification of FLUXNET sites has been performed to select only those
19 sites with the lower level of heterogeneity. Albedo measurements at the sites passing the selection are
20 in excellent agreement for most forest sites, while satellite retrievals underestimate *in situ*
21 measurements for PFTs with larger values of albedo (typically non-forest ecosystems as CRO and
22 GRA).

23 When seasonal patterns of MODIS albedo are compared, the match is extremely good for all forest
24 PFTs. These results quantitatively document the quality achieved with satellite retrievals of surface

1 albedo over a range of forest ecosystems. On the contrary, in non-forest sites satellite retrievals
2 systematically underestimate *in situ* measurements across the whole seasonal cycle with a minimum
3 error at the peak of the growing season. However, in the interpretation of these results it should be
4 considered that the footprint of the surface radiometric measurements is extremely limited in these
5 ecosystems, since sensors are generally installed few meters above the ground. In addition the temporal
6 and fine-scale spatial variability of the canopy reflectance can be extremely large in non-forest PFTs
7 due to management practices and rapid LAI dynamics (Tittebrand et al., 2009).

8 The intercomparison of surface measurements and satellite retrievals is affected by the surface
9 heterogeneity at various spatial scale. The sub-pixel variability affects the difference between the signal
10 in the footprint of the albedometer and the 500 m MODIS pixel, while the between pixels variability
11 affects the accuracy of the inversion algorithm. At smaller scale, the combination of quantitative
12 indexes based on variogram analysis of high resolution images confirms that FLUXNET sites in
13 herbaceous ecosystems (CRO and GRA) are the less homogenous and should therefore be carefully
14 evaluated in point to pixel intercomparisons. At a coarser scale, the variability of the MODIS albedo in
15 the 7x7 Km² area is related to the mismatch of MODIS retrievals and in situ measurements, further
16 corroborating the relevance of large scale landscape homogeneity in the comparison of surface
17 measurements and satellite retrievals.

18 The results of this investigation clearly show the need for the future to characterize the spatial
19 heterogeneity of reference sites using a combination of surface measurements, airborne and finer scale
20 satellite imagery (Román et al., 2009). To overcome the limitations of the point to pixel albedo inter-
21 comparisons, future field and airborne surveys should be planned to address the issue of spatial scales
22 and landscape heterogeneity. Current approaches for measuring in-situ albedo are not adequate to
23 describe mixed or highly heterogeneous landscapes such as mixed forests, open shrublands, savannas
24 and croplands. For this purpose only spatially-distributed measurements (i.e., airborne laser scanning,
25 network of tall towers) could produce observations at the required scale. For albedo in particular, multi-

1 angle airborne instruments such as AirMISR (Diner et al., 1998), AirPOLDER (Chen et al., 1997),
2 NASA's Cloud Absorption Radiometer (Gatebe et al., 2003) and the Compact Airborne Spectrographic
3 Imager (CASI) data (Chen et al., 1999) could be effectively used to retrieve surface-level bidirectional
4 reflectance measurements at landscape scale and therefore effectively complement moderate resolution
5 satellite systems like MODIS and MISR.

6

7 **Acknowledgments**

8 This work is based on radiometric measurements acquired by the FLUXNET community and in
9 particular by the following networks: AmeriFlux (U.S. Department of Energy, Biological and
10 Environmental Research, Terrestrial Carbon Program (DE-FG02-04ER63917 and DE-FG02-
11 04ER63911)), AfriFlux, AsiaFlux, CarboAfrica, CarboEuropeIP, CarboItaly, CarboMont, ChinaFlux,
12 FLUXNET-Canada (supported by CFCAS, NSERC, BIOCAP, Environment Canada, and NRCan),
13 GreenGrass, KoFlux, LBA, NECC, OzFlux, TCOS-Siberia, USCCC. We acknowledge the support to
14 data harmonization provided by CarboEuropeIP, FAO-GTOS-TCO, iLEAPS (the Integrated Land
15 Ecosystem-Atmosphere Processes Study, a core project of IGBP), Max Planck Institute for
16 Biogeochemistry, National Science Foundation, University of Tuscia, Université Laval and
17 Environment Canada and US Department of Energy and the database development and technical
18 support from Berkeley Water Center, Lawrence Berkeley National Laboratory, Microsoft Research
19 eScience, Oak Ridge National Laboratory, University of California - Berkeley, University of Virginia.
20 The processing of MODIS data has been supported by NASA grant NNX08AE94A.

21

1 **Figure captions**

2 Figure 1 – Spatial distribution of the 120 FLUXNET sites for which albedo measurements are
3 available. Green dots represent sites selected for the analysis according to plant cover
4 homogeneity at 1 Km² scale (n=53, visual classification based on high resolution Google
5 Earth™ images, e.g. Fig 2).

6 Figure 2 – Frequency distribution of synchronous MODIS retrievals and in situ measurements
7 classified according to year (panel a) and month (panel b) of observation. The vegetation is
8 coded according to the IGBP classification: CRO, croplands; CSH, closed shrublands; DBF,
9 deciduous broad-leaf forests; EBF, evergreen broad-leaf forests; ENF, evergreen needle-leaf
10 forests; GRA, grassland; MF, mixed forests; OSH, open shrublands; SAV, savannas; WET,
11 permanent wetlands; WSA, woody savannas. Validation sites are separated into forest (ENF,
12 EBF, DBF, MF, SAV and WSA) and non forest (OSH, CSH, CRO, GRA, WET).

13 Figure 3 – Global distribution of MODIS albedo (0.05° res.) categorized for latitudinal bands (panel a)
14 and Plant Functional Types (panel b). In both panels black dots represent global MODIS
15 averages (grey bars show the 10-90 percentile intervals) and white dots represent MODIS
16 retrievals at the 53 FLUXNET sites reported in Table 1.

17 Figure 4 – Examples of high resolution Google Earth™ images used to visually classify the FLUXNET
18 sites according to land cover homogeneity. Images cover an area of 1km² area centered at the
19 tower coordinates.

20 Figure 5 – Time series of synchronous in situ observations (open dots) and MODIS retrievals (black
21 dots) at the four sites shown in Fig. 4.

22 Figure 6 – MODIS retrievals *versus* in situ observations of clear-sky and snow-free albedo. a) Averages
23 and standard deviations of retrievals (temporal and spatial variability are accounted for)

1 grouped by Plant Functional Types (PFT), b) Average ground measurements and retrievals at
2 individual sites classified by PFT.

3 Figure 7 – Mean error and mean absolute error of MODIS albedo retrievals at FLUXNET sites. Site
4 numbers are reported in Table1; dot size is proportional to the R^2 of the regression of daily
5 MODIS retrievals *versus* in situ measurements.

6 Figure 8 – Mean absolute percentage error of MODIS retrievals versus in situ measurements as a
7 function of the standard deviation of MODIS retrievals in the 7x7 Km grid centered at the site.
8 Sites located in a more homogeneous landscape (lower spatial variability of albedo) are
9 characterized by a lower discrepancy between in situ observations and satellite retrievals.

10 Figure 9 – Seasonal average values of clear-sky snow-free albedo at the 53 homogeneous sites as
11 measured at the FLUXNET sites or retrieved from MODIS. Winter values (DJF) show the
12 lowest correlation. The first panel includes the correlation matrix of the residuals (MODIS
13 retrievals- in situ albedo) in the four seasons.

14 Figure 10 – Seasonal trends of albedo for the different plant functional types as derived from in situ
15 observations (white dots) and MODIS retrievals (black dots). The grey bands show the
16 observed variability (10-90 percentiles) of the MODIS retrieved albedo at global scale for each
17 plant functional type.

18

1 **References**

2 Alton, P. (2009). A simple retrieval of ground albedo and vegetation absorptance from MODIS satellite
3 data for parameterisation of global Land-Surface Models. *Agricultural and Forest Meteorology*, 149,
4 1769-1775.

5 Anderson, R.G., Canadell, J.G., Randerson, J.T., Jackson, R.B., Hungate, B.A., Baldocchi, D.D., Ban-
6 Weiss, G.A., Bonan, G.B., Caldeira, K., Cao, L., Diffenbaugh, N.S., Gurney, K.R., Kueppers, L.M.,
7 Law, B.E., Luyssaert, S., & O'Halloran, T.L. (2010). Biophysical considerations in forestry for climate
8 protection. *Frontiers in Ecology and the Environment*. doi:10.1890/090179.

9 Baldocchi, D., Falge, E., Gu, L., Olson, R., Hollinger, D., Running, S., Anthoni, P., Bernhofer, C.,
10 Davis, K., Evans, R., Fuentes, J., Goldstein, A., Katul, G., Law, B., Lee, X., Malhi, Y., Meyers, T.,
11 Munger, W., Oechel, W., Paw, K.T., Pilegaard, K., Schmid, H.P., Valentini, R., Verma, S., Vesala, T.,
12 Wilson, K., & Wofsy, S. (2001). FLUXNET: A New Tool to Study the Temporal and Spatial
13 Variability of Ecosystem-Scale Carbon Dioxide, Water Vapor, and Energy Flux Densities. *Bulletin of*
14 *the American Meteorological Society*, 82, 2415-2434. doi:10.1175/1520-0477.

15 Betts, R.A. (2000). Offset of the potential carbon sink from boreal forestation by decreases in surface
16 albedo. *Nature*, 408, 187-190.

17 Betts, R.A., Falloon, P.D., Goldewijk, K.K., & Ramankutty, N. (2007). Biogeophysical effects of land
18 use on climate: Model simulations of radiative forcing and large-scale temperature change.
19 *Agricultural and Forest Meteorology*, 142, 216-233.

20 Bird, D.N., Kunda, M., Mayer, A., Schlamadinger, B., Canella, L., & Johnston, M. (2008).
21 Incorporating changes in albedo in estimating the climate mitigation benefits of land use change
22 projects. *Biogeosciences Discuss.*, 5, 1511-1543.

1 Bonan, G.B. (2008). Forests and Climate Change: Forcings, Feedbacks, and the Climate Benefits of
2 Forests. *Science*, 320, 1444-1449.

3 Cescatti, A. (1998). Effects of needle clumping in shoots and crowns on the radiative regime of a
4 Norway spruce canopy. *Annals of Forest Science*, 55, 89-102.

5 Chapin, F.S., Randerson, J.T., McGuire, A.D., Foley, J.A., & Field, C.B. (2008). Changing feedbacks
6 in the climate-biosphere system. *Frontiers in Ecology and the Environment*, 6, 313-320.
7 doi:10.1890/080005.

8 Chapin, F.S., Sturm, M., Serreze, M.C., McFadden, J.P., Key, J.R., Lloyd, A.H., McGuire, A.D., Rupp,
9 T.S., Lynch, A.H., Schimel, J.P., Beringer, J., Chapman, W.L., Epstein, H.E., Euskirchen, E.S.,
10 Hinzman, L.D., Jia, G., Ping, C.L., Tape, K.D., Thompson, C.D.C., Walker, D.A., & Welker, J.M.
11 (2005). Role of land-surface changes in arctic summer warming. *Science*, 310, 657-660.

12 Charlson, R.J., Ackerman, A.S., Bender, F.A.M., Anderson, T.L., & Liu, Z. (2007). On the climate
13 forcing consequences of the albedo continuum between cloudy and clear air. *Tellus Series B-Chemical
14 and Physical Meteorology*, 59, 715-727. doi:10.1111/j.1600-0889.2007.00297.

15 Charney, J., Quirk, W.J., Chow, S.H., & Kornfield, J. (1977). A comparative study of the effects of
16 albedo change on drought in semi-arid regions. *Journal of the Atmospheric Sciences*, 34, 1366-1385.

17 Chen, J.M., Leblanc, S.G., Cihlar, J.C., Bicheron, P., Leroy, M., Deering, D., & Eck, T. (1997). Studies
18 of BRDF in conifer and deciduous boreal forests using the 4-scale model and airborne POLDER and
19 ground-based PARABOLA measurements. In, *Geoscience and Remote Sensing, 1997. IGARSS '97.
20 Remote Sensing - A Scientific Vision for Sustainable Development., 1997 IEEE International* (pp. 165-
21 167 vol.161)

1 Chen, J.M., Leblanc, S.G., Miller, J.R., Freemantle, J., Loechel, S.E., Walthall, C.L., Inanen, K.A., &
2 White, H.P. (1999). Compact Airborne Spectrographic Imager (CASI) used for mapping biophysical
3 parameters of boreal forests. *J. Geophys. Res.*, *104*, 27945-27958.

4 Chen, Y.M., Liang, S., Wang, J., Kim, H.Y., & Martonchik, J.V. (2008). Validation of MISR land
5 surface broadband albedo. *International Journal of Remote Sensing*, *29*, 6971-6983.
6 10.1080/01431160802199876.

7 Davidson, A., & Wang, S.S. (2004). The effects of sampling resolution on the surface albedos of
8 dominant land cover types in the North American boreal region. *Remote Sensing of Environment*, *93*,
9 211-224. 10.1016/j.rse.2004.07.005.

10 Dickinson, R.E. (1983). Land surface processes and climate surface albedos and energy-balance.
11 *Advances in Geophysics*, *25*, 305-353.

12 Diner, D.J., Barge, L.M., Bruegge, C.J., Chrien, T.G., Conel, J.E., Eastwood, M.L., Garcia, J.D.,
13 Hernandez, M.A., Kurzweil, C.G., Ledebor, W.C., Pignatano, N.D., Sarture, C.M., & Smith, B.G.
14 (1998). The Airborne Multi-angle Imaging SpectroRadiometer (AirMISR): instrument description and
15 first results. *Geoscience and Remote Sensing, IEEE Transactions on*, *36*, 1339-1349.

16 Dirmeyer, P.A., & Shukla, J. (1994). Albedo as a modulator of climate response to tropical
17 deforestation. *Journal Geophysical Research*, *99*, 20863-20877.

18 Frida A-M, B., Henning, R., Robert J, C., Annica M. L, E., & Norman, L. (2006). 22 views of the
19 global albedo - comparison between 20 GCMs and two satellites. *Tellus A*, *58*, 320-330.

20 Gao, F., Schaaf, C.B., Strahler, A.H., Roesch, A., Lucht, W., & Dickinson, R. (2005). MODIS
21 bidirectional reflectance distribution function and albedo Climate Modeling Grid products and the

1 variability of albedo for major global vegetation types. *Journal of Geophysical Research-Atmospheres*,
2 110, D01104. doi:10.1029/2004jd005190.

3 Gatebe, C.K., King, M.D., Platnick, S., Arnold, G.T., Vermote, E.F., & Schmid, B. (2003). Airborne
4 spectral measurements of surface and atmosphere anisotropy for several surfaces and ecosystems
5 over southern Africa. *J. Geophys. Res.*, 108, 8489.

6 Govaerts, Y., & Lattanzio, A. (2008). Estimation of surface albedo increase during the eighties Sahel
7 drought from Meteosat observations. *Global and Planetary Change*, 64, 139-145.

8 Hall, A., & Qu, X. (2006). Using the current seasonal cycle to constrain snow albedo feedback in future
9 climate change. *Geophysical Research Letters*, 33. doi:10.1029/2005gl025127.

10 Henderson-Sellers, A., & Wilson, M.F. (1983). Surface albedo data for climatic modeling. *Reviews of*
11 *Geophysics*, 21, 1743-1778.

12 Holben, B.N., Eck, T.F., Slutsker, I., Tanré, D., Buis, J.P., Setzer, A., Vermote, E., Reagan, J.A.,
13 Kaufman, Y.J., Nakajima, T., Lavenu, F., Jankowiak, I., & Smirnov, A. (1998). AERONET--A
14 Federated Instrument Network and Data Archive for Aerosol Characterization. *Remote Sensing of*
15 *Environment*, 66, 1-16.

16 Hollinger, D.Y., Ollinger, S.V., Richardson, A.D., Meyers, T.P., Dail, D.B., Martin, M.E., Scott, N.A.,
17 Arkebauer, T.J., Baldocchi, D.D., Clark, K.L., Curtis, P.S., Davis, K.J., Desai, A.R., Dragoni, D.,
18 Goulden, M.L., Gu, L., Katul, G.G., Pallardy, S.G., PawU, K.T., Schmid, H.P., Stoy, P.C., Suyker,
19 A.E., & Verma, S.B. (2009). Albedo estimates for land surface models and support for a new paradigm
20 based on foliage nitrogen concentration. *Global Change Biology*, 16, 696-710.

1 Jin, Y., Schaaf, C.B., Woodcock, C.E., Gao, F., Li, X., Strahler, A.H., Lucht, W., & Liang, S. (2003a).
2 Consistency of MODIS surface bidirectional reflectance distribution function and albedo retrievals: 2.
3 Validation. *Journal Geophysical Research*, 108. doi:10.1029/2002JD002804.

4 Jin, Y.F., Schaaf, C.B., Gao, F., Li, X.W., Strahler, A.H., Lucht, W., & Liang, S.L. (2003b).
5 Consistency of MODIS surface bidirectional reflectance distribution function and albedo retrievals: 1.
6 Algorithm performance. *Journal of Geophysical Research-Atmospheres*, 108.
7 doi:10.1029/2002jd002803.

8 Lawrence, D.M., & Slingo, J.M. (2004). An annual cycle of vegetation in a GCM. Part II: global
9 impacts on climate and hydrology. *Climate Dynamics*, 22, 107-122. doi:10.1007/s00382-003-0367-8.

10 Liang, S.L., Fang, H.L., Chen, M.Z., Shuey, C.J., Walthall, C., Daughtry, C., Morisette, J., Schaaf, C.,
11 & Strahler, A. (2002). Validating MODIS land surface reflectance and albedo products: methods and
12 preliminary results. *Remote Sensing of Environment*, 83, 149-162.

13 Liu, J., Schaaf, C., Strahler, A., Jiao, Z., Shuai, Y., Zhang, Q., Roman, M., Augustine, J.A., & Dutton,
14 E.G. (2009). Validation of Moderate Resolution Imaging Spectroradiometer (MODIS) albedo retrieval
15 algorithm: Dependence of albedo on solar zenith angle. *Journal Geophysical Research*, 114, D01106.

16 Lucht, W., Hyman, A.H., Strahler, A.H., Barnsley, M.J., Hobson, P., & Muller, J.P. (2000a). A
17 Comparison of Satellite-Derived Spectral Albedos to Ground-Based Broadband Albedo Measurements
18 Modeled to Satellite Spatial Scale for a Semidesert Landscape. *Remote Sensing of Environment*, 74, 85-
19 98.

20 Lucht, W., Schaaf, C.B., & Strahler, A.H. (2000b). An algorithm for the retrieval of albedo from space
21 using semiempirical BRDF models. *IEEE transactions on geoscience and remote sensing*, 38, 977-998.

1 Masuoka, E., Tilmes, C., Gang, Y., & Devine, N. (2000). Producing global science products for the
2 MODerate resolution Imaging Spectroradiometer (MODIS) in MODAPS. In, *Geoscience and Remote*
3 *Sensing Symposium, 2000. Proceedings. IGARSS 2000. IEEE 2000 International* (pp. 2050-2052
4 vol.2055)

5 Masuoka, E., Wolfe, R., Sinno, S., Gang, Y., & Teague, M. (2007). A disk-based system for producing
6 and distributing science products from MODIS. In, *Geoscience and Remote Sensing Symposium, 2007.*
7 *IGARSS 2007. IEEE International* (pp. 3043-3046)

8 Moody, Eric, G., King, Michael, D., Schaaf, Crystal, B., Platnick, & Steven, G. (2008). MODIS-
9 Derived Spatially Complete Surface Albedo Products : Spatial and Temporal Pixel Distribution and
10 Zonal Averages. *Journal of Applied Meteorology and Climatology*, 47, 2879-2894.

11 Myhre, G., Kvalevåg, M.M., & Schaaf, C.B. (2005). Radiative forcing due to anthropogenic vegetation
12 change based on MODIS surface albedo data. *Geophysical Research Letters*, 32, L21410.

13 Ollinger, S.V., Richardson, A.D., Martin, M.E., Hollinger, D.Y., Froking, S.E., Reich, P.B., Plourde,
14 L.C., Katul, G.G., Munger, J.W., Oren, R., Smith, M.L., Paw U, K.T., Bolsta, P.V., Cook, B.D., Day,
15 M.C., Martin, T.A., Monson, R.K., & Schmid, H.P. (2008). Canopy nitrogen, carbon assimilation, and
16 albedo in temperate and boreal forests: Functional relations and potential climate feedbacks.
17 *Proceedings of the National Academy of Sciences of the United States of America*, 105, 19336-19341.

18 Pinty, B., Andredakis, I., Clerici, M., Kaminski, T., Taberner, M., Verstraete, M.M., Gobron, N.,
19 Plummer, S., & Widlowski, J.L. (2011a). Exploiting the MODIS albedos with the Two-stream
20 Inversion Package (JRC-TIP): 1. Effective leaf area index, vegetation, and soil properties. *J. Geophys.*
21 *Res.*, 116, D09105.

1 Pinty, B., Taberner, M., Haemmerle, V.R., Paradise, S.R., Vermote, E., Verstraete, M.M., Gobron, N.,
2 & Widlowski, J.-L. (2011b). Global-Scale Comparison of MISR and MODIS Land Surface Albedos.
3 *Journal of Climate*, 24, 732-749. doi:10.1175/2010JCLI3709.1.

4 Pirazzini, R. (2004). Surface albedo measurements over Antarctic sites in summer. *J. Geophys. Res.*,
5 109, D20118.

6 Pirazzini, R., Vihma, T., Granskog, M.A., & Cheng, B. (2006). Surface albedo measurements over sea
7 ice in the Baltic Sea during the spring snowmelt period. *Annals of Glaciology*, 44, 7-14.

8 Randerson, J.T., Liu, H., Flanner, M.G., Chambers, S.D., Jin, Y., Hess, P.G., Pfister, G., Mack, M.C.,
9 Treseder, K.K., Welp, L.R., Chapin, F.S., Harden, J.W., Goulden, M.L., Lyons, E., Neff, J.C., Schuur,
10 E.A.G., & Zender, C.S. (2006). The Impact of Boreal Forest Fire on Climate Warming. *Science*, 314,
11 1130-1132. doi:10.1126/science.1132075.

12 Román, M.O., Schaaf, C.B., Lewis, P., Gao, F., Anderson, G.P., Privette, J.L., Strahler, A.H.,
13 Woodcock, C.E., & Barnsley, M. (2010). Assessing the coupling between surface albedo derived from
14 MODIS and the fraction of diffuse skylight over spatially-characterized landscapes. *Remote Sensing of*
15 *Environment*, 114, 738-760.

16 Román, M.O., Schaaf, C.B., Woodcock, C.E., Strahler, A.H., Yang, X., Braswell, R.H., Curtis, P.S.,
17 Davis, K.J., Dragoni, D., Goulden, M.L., Gu, L., Hollinger, D.Y., Kolb, T.E., Meyers, T.P., Munger,
18 J.W., Privette, J.L., Richardson, A.D., Wilson, T.B., & Wofsy, S.C. (2009). The MODIS (Collection
19 V005) BRDF/albedo product: Assessment of spatial representativeness over forested landscapes.
20 *Remote Sensing of Environment*, 113, 2476-2498.

21 Rotenberg, E., & Yakir, D. (2010). Contribution of Semi-Arid Forests to the Climate System. *Science*,
22 327, 451-454. doi:10.1126/science.1179998.

1 Running, S.W., Loveland, T.R., Pierce, L.L., Nemani, R.R., & Hunt, E.R. (1995). A remote sensing
2 based vegetation classification logic for global land cover analysis. *Remote Sensing of Environment*,
3 *51*, 39-48.

4 Salomon, J., G., Schaaf, C., B., Strahler, A., H., Feng, G.A.O., & Yufang Jin, G. (2006). Validation of
5 the MODIS bidirectional reflectance distribution function and albedo retrievals using combined
6 observations from the Aqua and Terra platforms. *IEEE transactions on geoscience and remote sensing*,
7 *44*, 1908-1925.

8 Salomonson, V.V., Barnes, W.L., Maymon, P.W., Montgomery, H.E., & Ostrow, H. (1989). MODIS -
9 advanced facility instrument for studies of the earth as a system. *IEEE transactions on geoscience and*
10 *remote sensing*, *27*, 145-153.

11 Schaaf, C.B., Gao, F., Strahler, A.H., Lucht, W., Li, X.W., Tsang, T., Strugnell, N.C., Zhang, X.Y., Jin,
12 Y.F., Muller, J.P., Lewis, P., Barnsley, M., Hobson, P., Disney, M., Roberts, G., Dunderdale, M., Doll,
13 C., d'Entremont, R.P., Hu, B.X., Liang, S.L., Privette, J.L., & Roy, D. (2002). First operational BRDF,
14 albedo nadir reflectance products from MODIS. *Remote Sensing of Environment*, *83*, 135-148.

15 Sellers, P.J., Hall, F.G., Kelly, R.D., Black, A., Baldocchi, D., Berry, J., Ryan, M., Ranson, K.J., Crill,
16 P.M., Lettenmaier, D.P., Margolis, H., Cihlar, J., Newcomer, J., Fitzjarrald, D., Jarvis, P.G., Gower,
17 S.T., Halliwell, D., Williams, D., Goodison, B., Wickland, D.E., & Guertin, F.E. (1997). BOREAS in
18 1997: Experiment overview, scientific results, and future directions. *Journal of Geophysical Research-*
19 *Atmospheres*, *102*, 28731-28769.

20 Stroeve, J., Box, J.E., Gao, F., Liang, S., Nolin, A., & Schaaf, C. (2005). Accuracy assessment of the
21 MODIS 16-day albedo product for snow: comparisons with Greenland in situ measurements. *Remote*
22 *Sensing of Environment*, *94*, 46-60.

1 Susaki, J., Yasuoka, Y., Kajiwara, K., Honda, Y., & Hara, K. (2007). Validation of MODIS Albedo
2 Products of Paddy Fields in Japan. *Geoscience and Remote Sensing, IEEE Transactions on*, 45, 206-
3 217.

4 Tian, Y., Dickinson, R.E., Zhou, L., Myneni, R.B., Friedl, M., Schaaf, C.B., Carroll, M., & Gao, F.
5 (2004). Land boundary conditions from MODIS data and consequences for the albedo of a climate
6 model. *Geophysical Research Letters*, 31, L05504.

7 Tittebrand, A., Spank, U., & Bernhofer, C.H. (2009). Comparison of satellite- and ground-based NDVI
8 above different land-use types. *Theoretical and Applied Climatology*, 98, 171-186.

9 Vavrus, S., Ruddiman, W.F., & Kutzbach, J.E. (2008). Climate model tests of the anthropogenic
10 influence on greenhouse-induced climate change: the role of early human agriculture, industrialization,
11 and vegetation feedbacks. *Quaternary Science Reviews*, 27, 1410-1425.

12 Wang, K., Liang, S., Schaaf, C.L., & Strahler, A.H. (2010). Evaluation of Moderate Resolution
13 Imaging Spectroradiometer land surface visible and shortwave albedo products at FLUXNET sites.
14 *Journal Geophysical Research*, 115, D17107.

15

16

Table 1 - Site characteristics derived from the FLUXNET database. *N obs* indicates the number of days of synchronous recordings of MODIS and in situ albedo. The averages of MODIS retrievals and in situ observations are reported in the two rightmost columns.

| N | SITE ID | COUNTRY | PFT | Lat. [deg] | Long. [deg] | N obs | MODIS albedo | In situ albedo | ST _{score} |
|----|---------|----------------|-----|---------------|----------------|-------|-----------------|-------------------|---------------------|
| 1 | AU Tum | Australia | EBF | -35.66 | 148.15 | 733 | 0.11 | 0.11 | 9.75 |
| 2 | AU Wac | Australia | EBF | -37.43 | 145.19 | 275 | 0.09 | 0.10 | 11.30 |
| 3 | BR Cax | Brazil | EBF | -1.72 | -51.46 | 67 | 0.12 | 0.12 | 5.33 |
| 4 | BR Sa3 | Brazil | EBF | -3.02 | -54.97 | 79 | 0.13 | 0.12 | 6.23 |
| 5 | BW Ghg | Botswana | SAV | -21.51 | 21.74 | 28 | 0.16 | 0.18 | 0.67 |
| 6 | BW Ghm | Botswana | WSA | -21.20 | 21.75 | 28 | 0.18 | 0.17 | NA |
| 7 | BW Ma1 | Botswana | WSA | -19.92 | 23.56 | 252 | 0.16 | 0.14 | 5.42 |
| 8 | CA Ca1 | Canada | ENF | 49.87 | -125.33 | 580 | 0.09 | 0.09 | 5.99 |
| 9 | CA Ca3 | Canada | ENF | 49.53 | -124.90 | 552 | 0.13 | 0.14 | 0.64 |
| 10 | CA NS6 | Canada | OSH | 55.92 | -98.96 | 353 | 0.10 | 0.12 | NA |
| 11 | CA SF2 | Canada | ENF | 54.25 | -105.88 | 363 | 0.11 | 0.11 | 1.72 |
| 12 | CA SF3 | Canada | ENF | 54.09 | -106.01 | 362 | 0.10 | 0.10 | 3.14 |
| 13 | CA WP1 | Canada | MF | 54.95 | -112.47 | 353 | 0.11 | 0.13 | 1.65 |
| 14 | CZ BK1 | Czech Republic | ENF | 49.50 | 18.54 | 148 | 0.09 | 0.10 | 3.18 |
| 15 | DE Geb | Germany | CRO | 51.10 | 10.91 | 328 | 0.17 | 0.18 | 0.90 |
| 16 | DE Hai | Germany | DBF | 51.08 | 10.45 | 451 | 0.13 | 0.13 | 1.97 |
| 17 | DE Kli | Germany | CRO | 50.89 | 13.52 | 256 | 0.16 | 0.19 | 0.62 |
| 18 | DE Tha | Germany | ENF | 50.96 | 13.57 | 477 | 0.10 | 0.07 | 5.99 |
| 19 | DE Wet | Germany | ENF | 50.45 | 11.46 | 375 | 0.07 | 0.05 | 1.55 |
| 20 | ES ES2 | Spain | CRO | 39.28 | -0.32 | 298 | 0.14 | 0.13 | 0.91 |
| 21 | ES LMa | Spain | SAV | 39.94 | -5.77 | 455 | 0.16 | 0.19 | 1.89 |
| 22 | FR Fon | France | DBF | 48.48 | 2.78 | 162 | 0.14 | 0.13 | 0.51 |
| 23 | FR Hes | France | DBF | 48.67 | 7.07 | 474 | 0.15 | 0.14 | 1.44 |
| 24 | FR Pue | France | EBF | 43.74 | 3.60 | 401 | 0.11 | 0.12 | 0.87 |
| 25 | GF Guy | French Guyana | EBF | 5.28 | -52.93 | 216 | 0.12 | 0.10 | 1.92 |
| 26 | HU Bug | Hungary | GRA | 46.69 | 19.60 | 523 | 0.16 | 0.20 | 1.74 |
| 27 | IE Dri | Ireland | GRA | 51.99 | -8.75 | 160 | 0.20 | 0.22 | 1.05 |
| 28 | IT Bon | Italy | ENF | 39.48 | 16.54 | 174 | 0.10 | 0.08 | 2.43 |
| 29 | IT Col | Italy | DBF | 41.85 | 13.59 | 183 | 0.14 | 0.15 | 2.60 |
| 30 | IT SRo | Italy | ENF | 43.73 | 10.28 | 512 | 0.08 | 0.09 | 3.10 |
| 31 | JP Mas | Japan | CRO | 36.05 | 140.03 | 177 | 0.12 | 0.13 | 1.15 |
| 32 | KR Kw1 | Korea | MF | 37.75 | 127.16 | 216 | 0.09 | 0.09 | 3.81 |
| 33 | NL Ca1 | Netherlands | GRA | 51.97 | 4.93 | 369 | 0.17 | 0.22 | 1.03 |
| 34 | NL Lan | Netherlands | CRO | 51.95 | 4.90 | 108 | 0.17 | 0.18 | 1.44 |
| 35 | NL Loo | Netherlands | ENF | 52.17 | 5.74 | 404 | 0.11 | 0.09 | 1.40 |
| 36 | PT Esp | Portugal | EBF | 38.64 | -8.60 | 437 | 0.13 | 0.11 | 0.86 |
| 37 | RU Che | Russia | MF | 68.61 | 161.34 | 104 | 0.15 | 0.16 | 0.54 |
| 38 | SE Nor | Sweden | ENF | 60.09 | 17.48 | 234 | 0.10 | 0.09 | 3.84 |
| 39 | UK Gri | UK | ENF | 56.61 | -3.80 | 15 | 0.10 | 0.09 | 1.48 |
| 40 | US Aud | USA | GRA | 31.59 | -110.51 | 1244 | 0.18 | 0.21 | 0.62 |
| 41 | US Bn1 | USA | ENF | 63.92 | -145.38 | 104 | 0.11 | 0.09 | 0.56 |
| 42 | US Bo1 | USA | CRO | 40.01 | -88.29 | 721 | 0.16 | 0.19 | NA |
| 43 | US Bo2 | USA | CRO | 40.01 | -88.29 | 289 | 0.16 | 0.19 | NA |
| 44 | US Fmf | USA | ENF | 35.14 | -111.73 | 247 | 0.10 | 0.12 | 3.08 |
| 45 | US FPe | USA | GRA | 48.31 | -105.10 | 775 | 0.15 | 0.16 | 1.05 |
| 46 | US Fuf | USA | ENF | 35.09 | -111.76 | 231 | 0.10 | 0.13 | 1.72 |
| 47 | US IB1 | USA | CRO | 41.86 | -88.22 | 349 | 0.15 | 0.16 | 0.76 |
| 48 | US Ivo | USA | WET | 68.49 | -155.75 | 62 | 0.18 | 0.19 | NA |
| 49 | US MMS | USA | DBF | 39.32 | -86.41 | 639 | 0.13 | 0.13 | 8.75 |
| 50 | US MOz | USA | DBF | 38.74 | -92.20 | 563 | 0.12 | 0.11 | 2.17 |
| 51 | US SRM | USA | WSA | 31.82 | -110.87 | 826 | 0.17 | 0.16 | 2.13 |
| 52 | US WCr | USA | DBF | 45.81 | -90.08 | 487 | 0.14 | 0.15 | 1.82 |
| 53 | ZA Kru | South Africa | SAV | -25.02 | 31.50 | 447 | 0.15 | 0.15 | 1.34 |

Table 2 – PFT averages of mean albedo (ground observation and satellite retrievals) and geostatistical indexes of landscape heterogeneity based on Landsat images. The analysis is limited to the 48 sites with available Landsat7 images. Records are shown in descending order of ST_{score} .

| PFT | N sites | MODIS | <i>In-situ</i> | MAE | R_{CV} | R_{SE} | R_{SV} | R_{ST} | ST_{score} |
|------------|----------------|--------------|-----------------------|------------|-----------------------|-----------------------|-----------------------|-----------------------|---------------------------|
| EBF | 7 | 0.115 | 0.109 | 0.014 | 17% | 20% | -3% | 48% | 5.18 |
| WSA | 2 | 0.167 | 0.148 | 0.020 | 14% | 52% | 31% | -3% | 3.77 |
| DBF | 7 | 0.138 | 0.136 | 0.013 | 42% | 15% | 78% | 10% | 2.75 |
| ENF | 15 | 0.100 | 0.095 | 0.017 | 24% | 23% | 44% | 17% | 2.65 |
| MF | 3 | 0.115 | 0.126 | 0.016 | 41% | 39% | 41% | 56% | 2.00 |
| SAV | 3 | 0.158 | 0.174 | 0.017 | 9% | 58% | 61% | -13% | 1.30 |
| GRA | 5 | 0.172 | 0.203 | 0.033 | 13% | 82% | 63% | -1% | 1.10 |
| CRO | 6 | 0.155 | 0.164 | 0.020 | 11% | 85% | 7% | 24% | 0.96 |

Figure 1

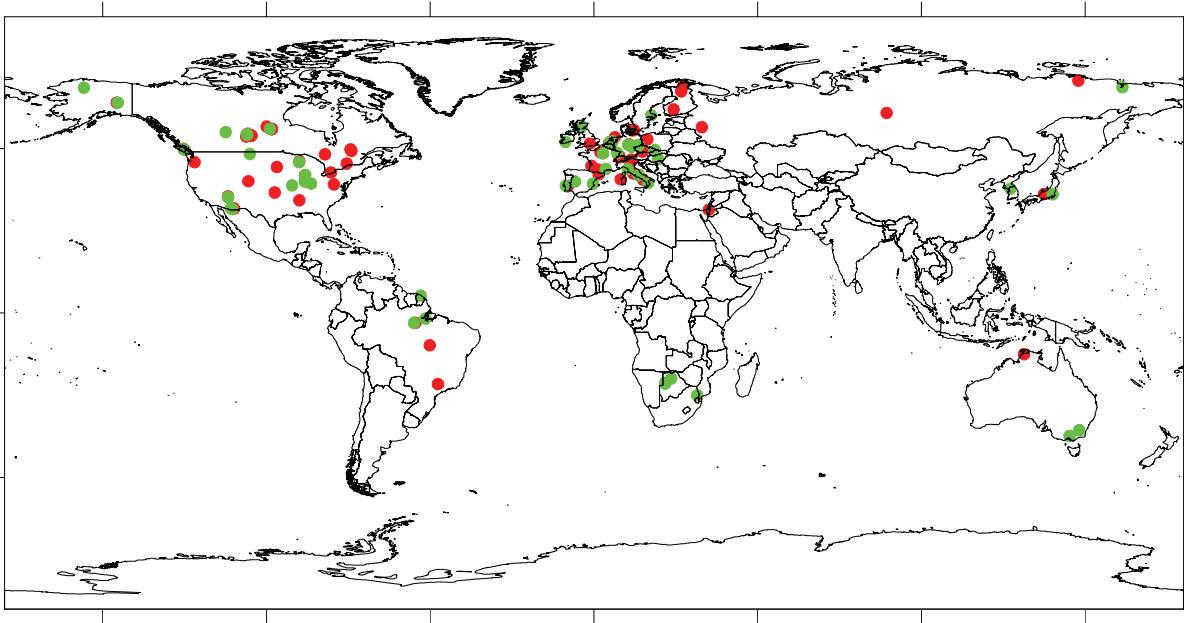


Figure 2

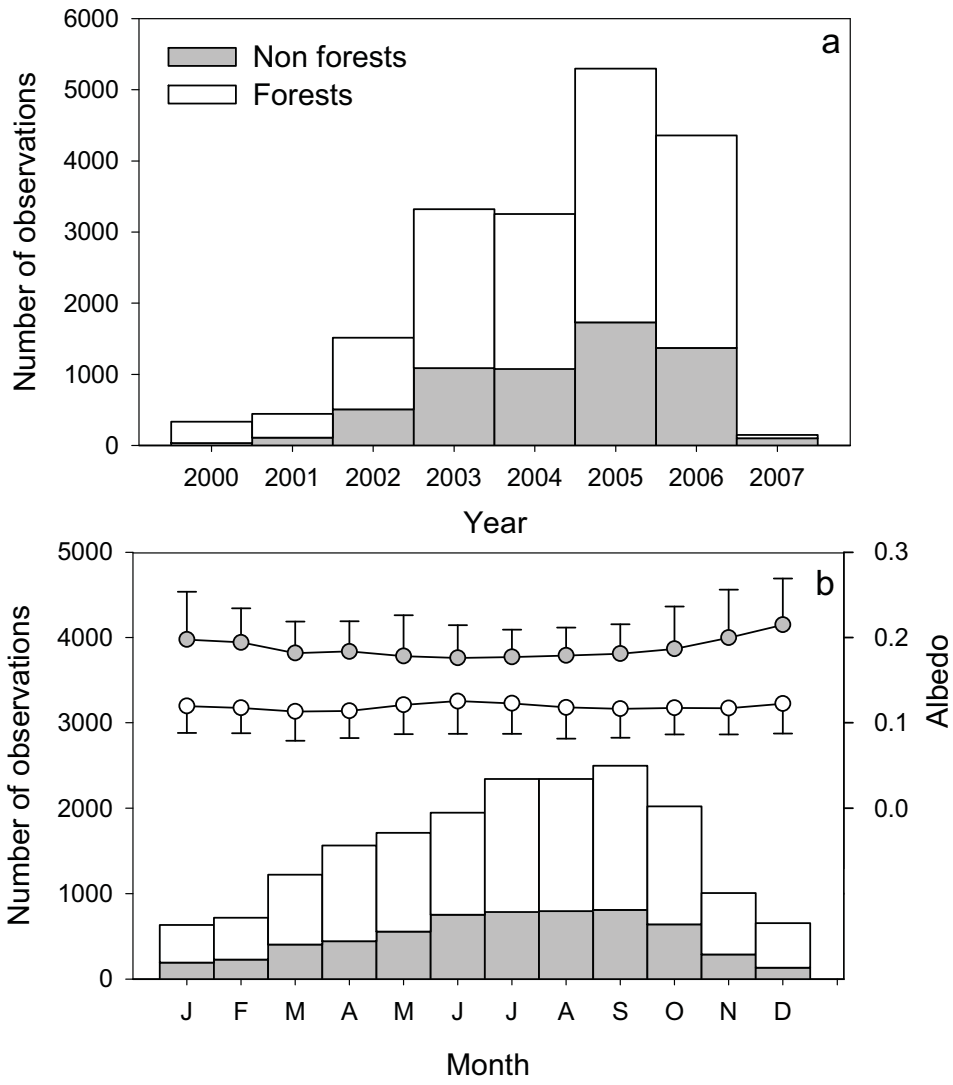


Figure 3

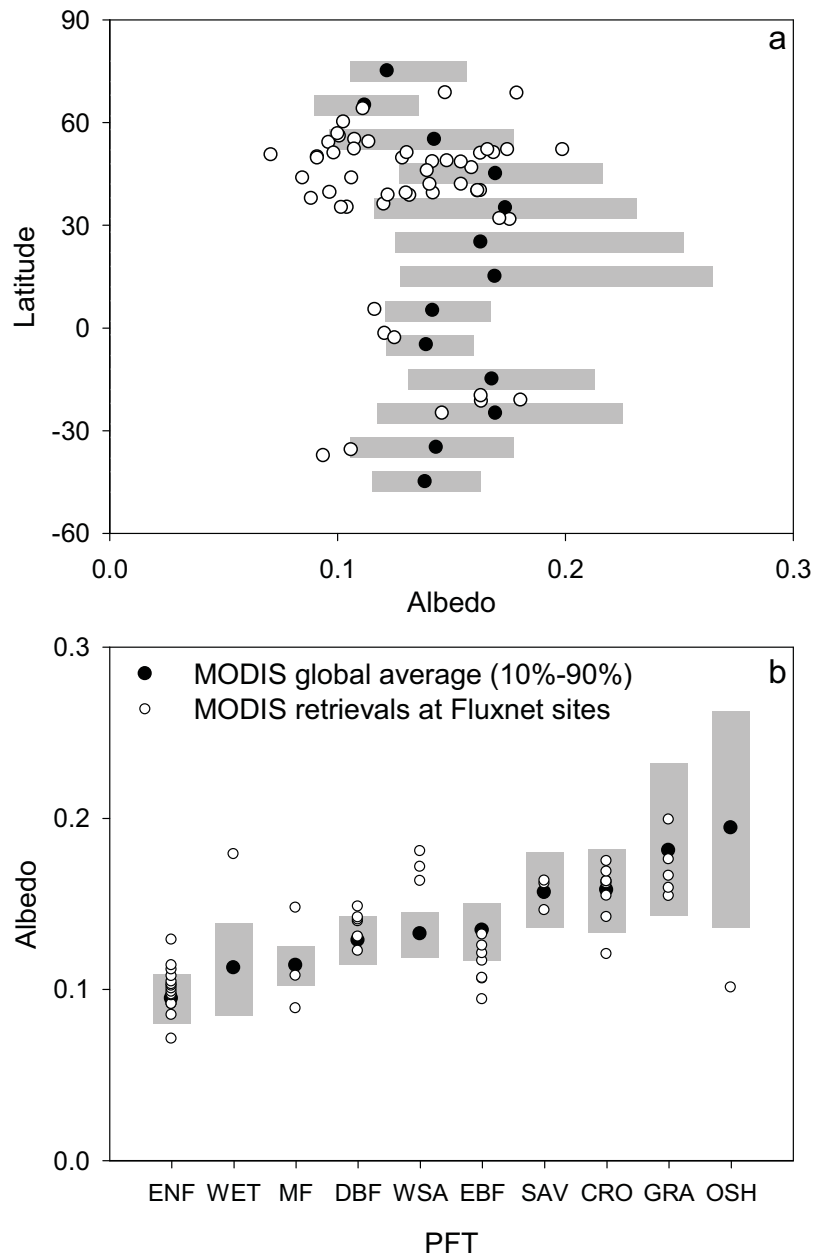


Figure 4

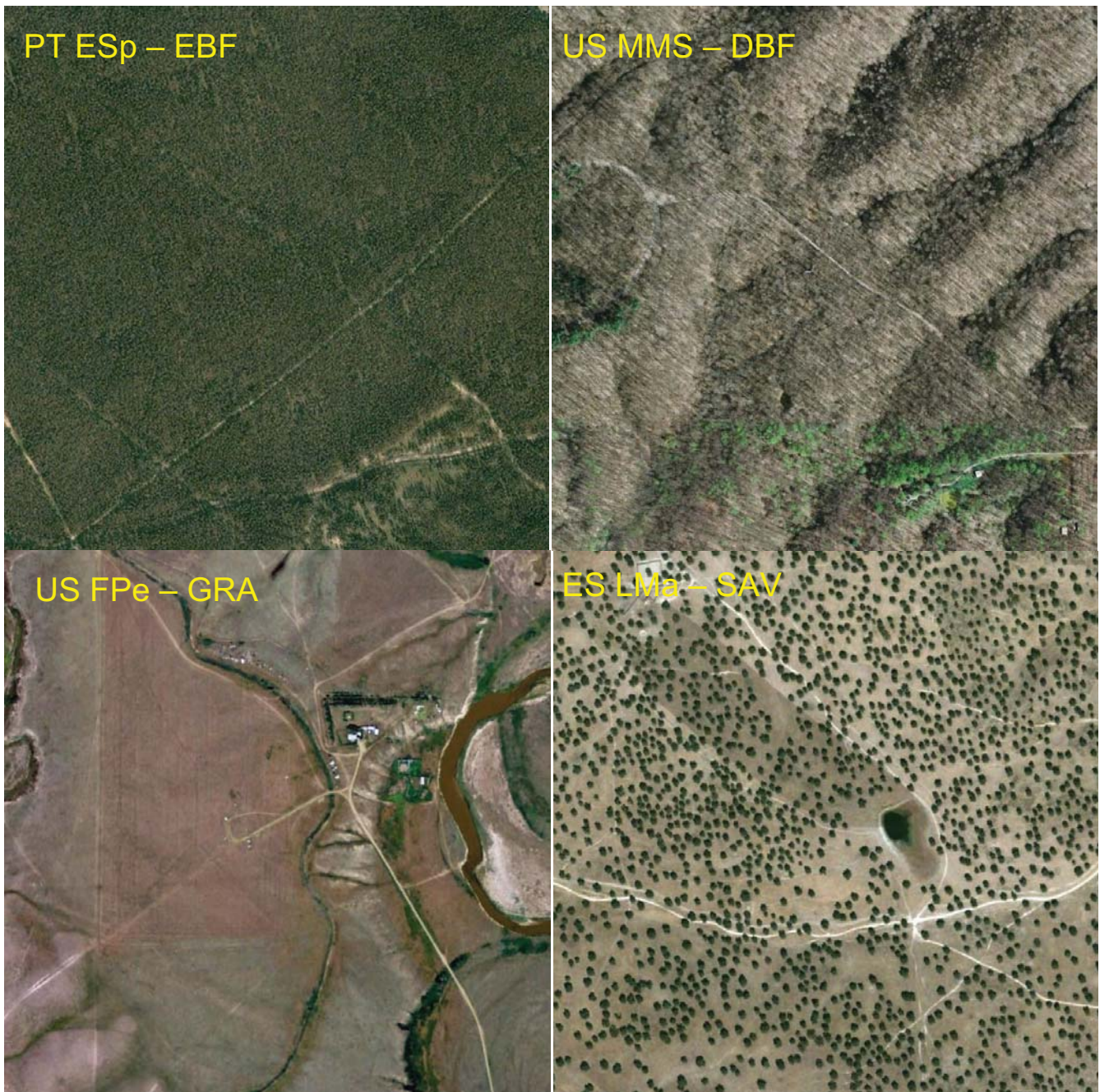


Figure 5

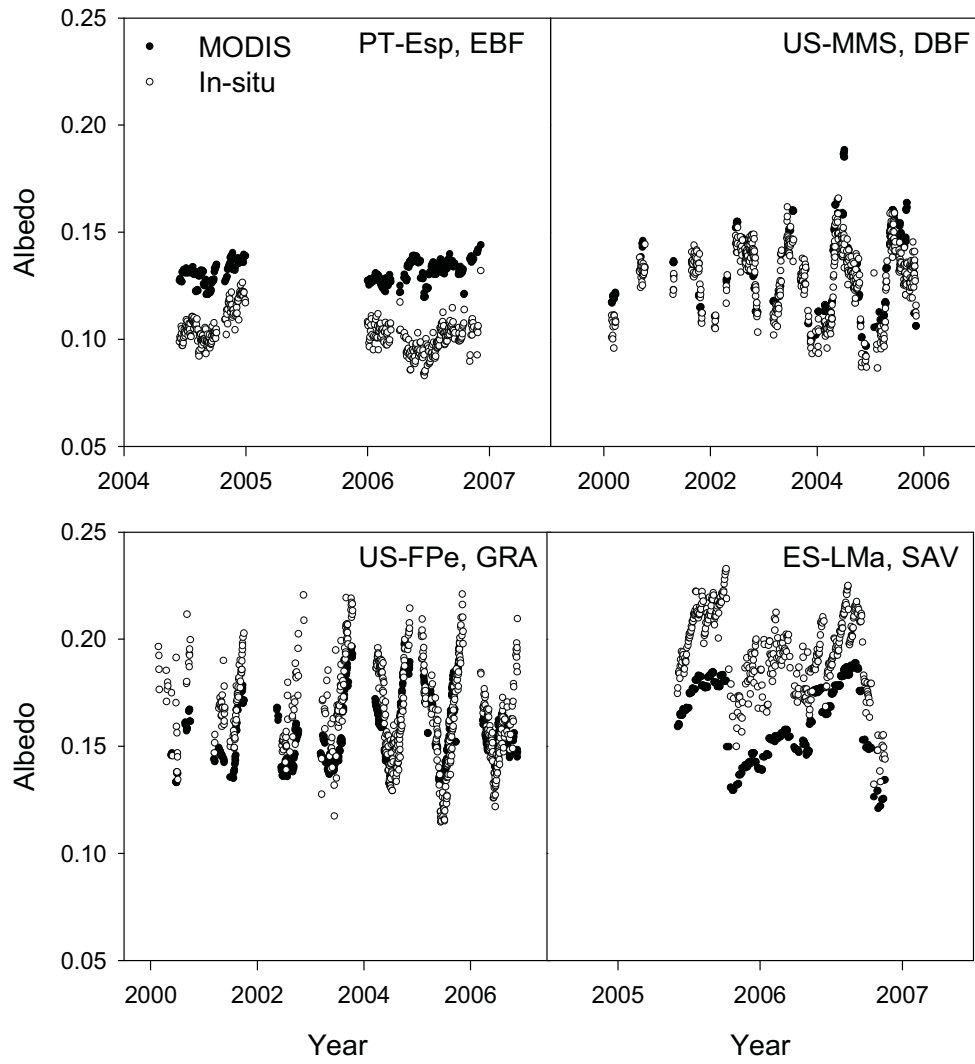


Figure 6

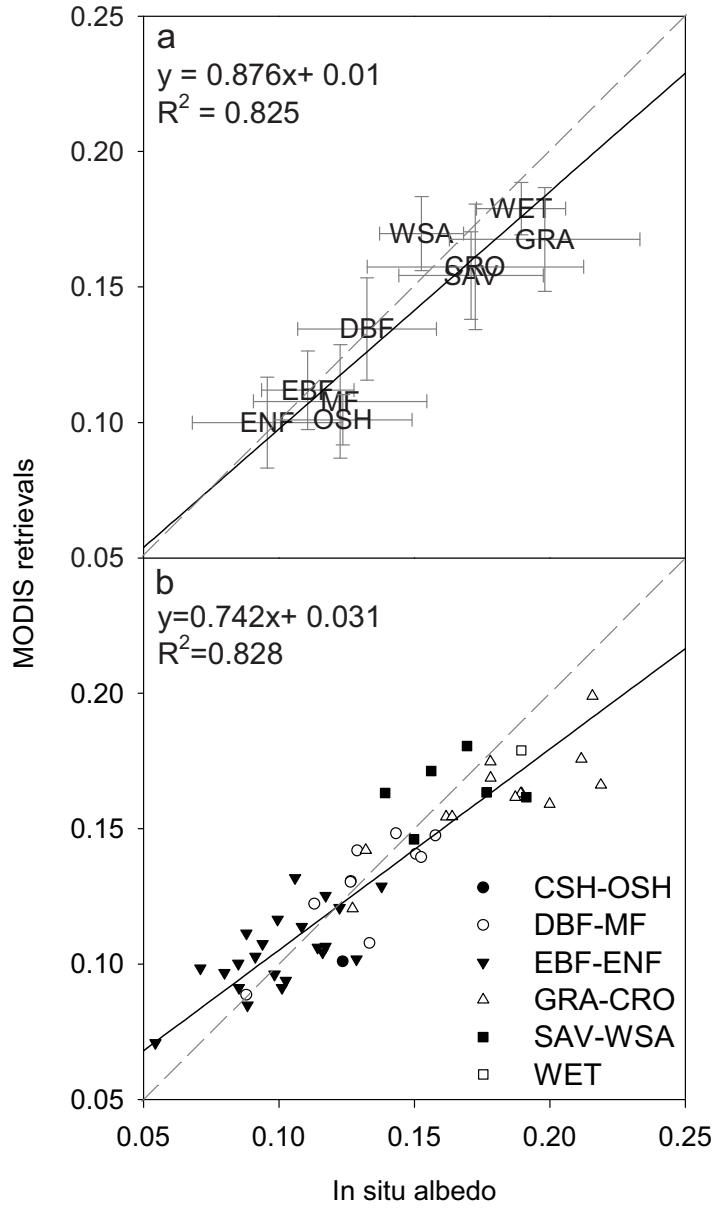


Figure 7

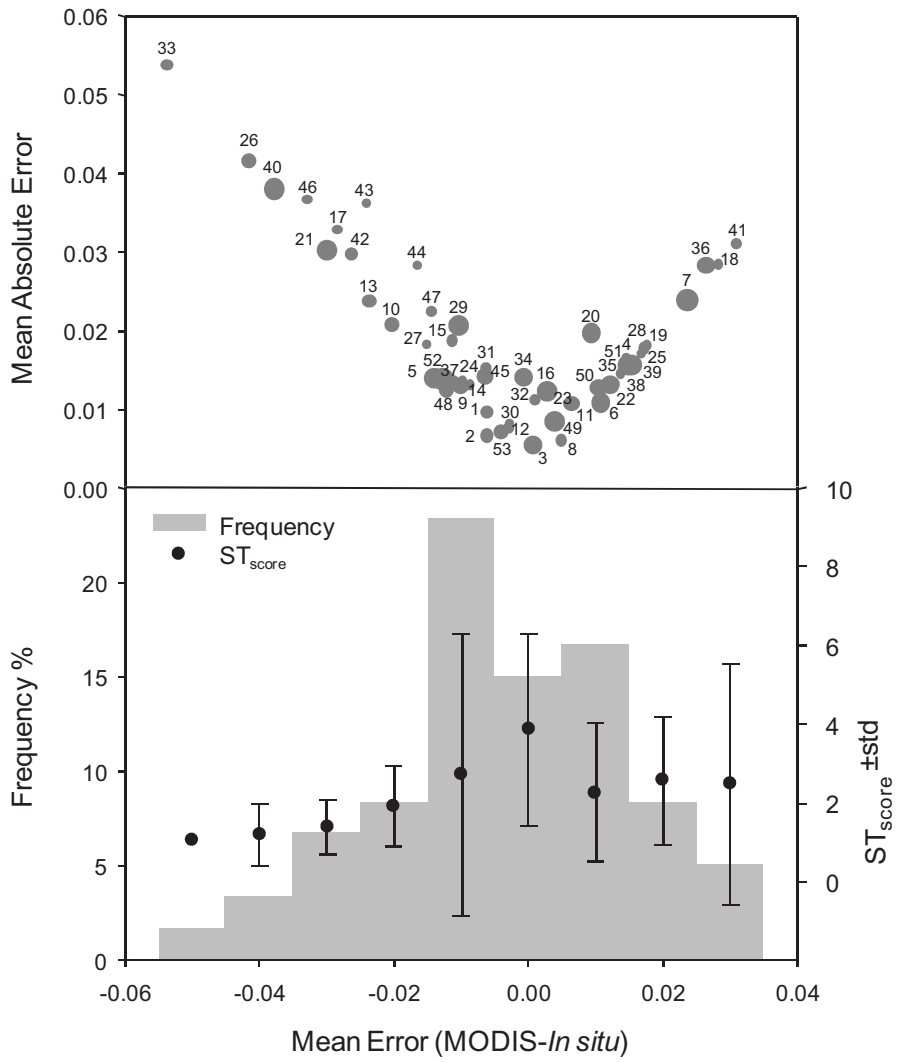


Figure 8

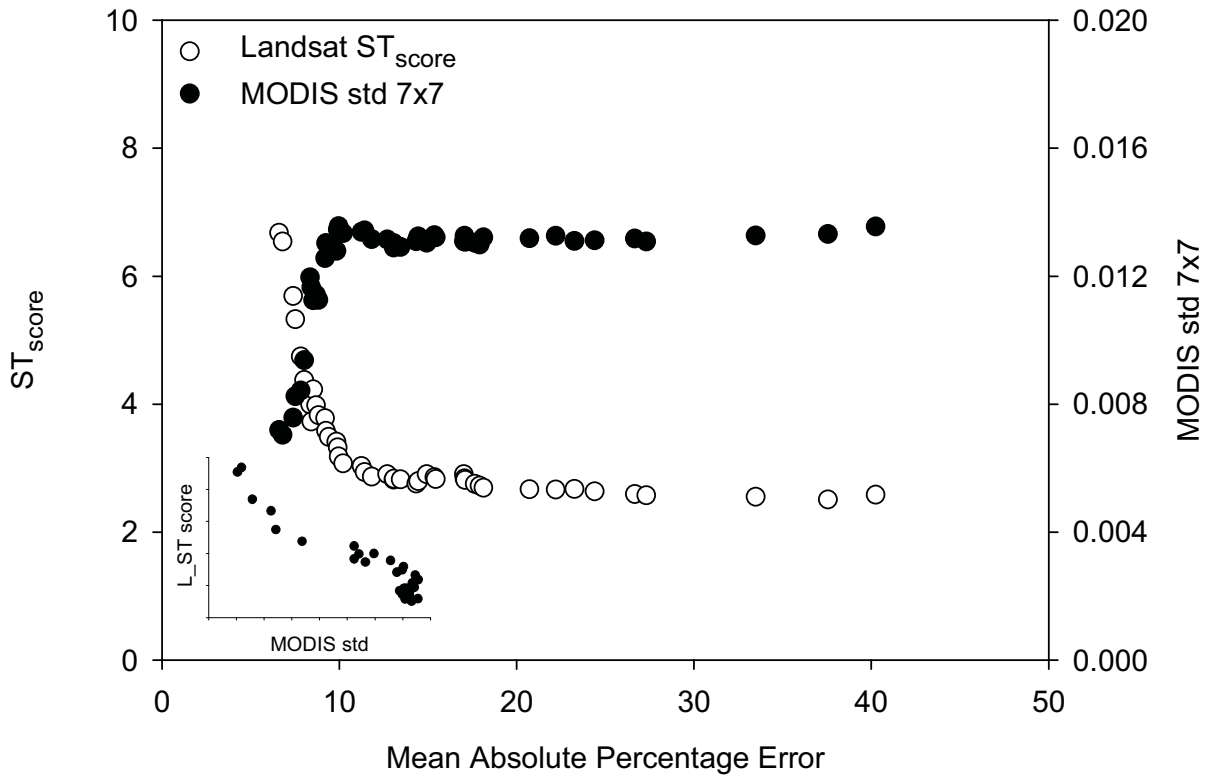


Figure 9

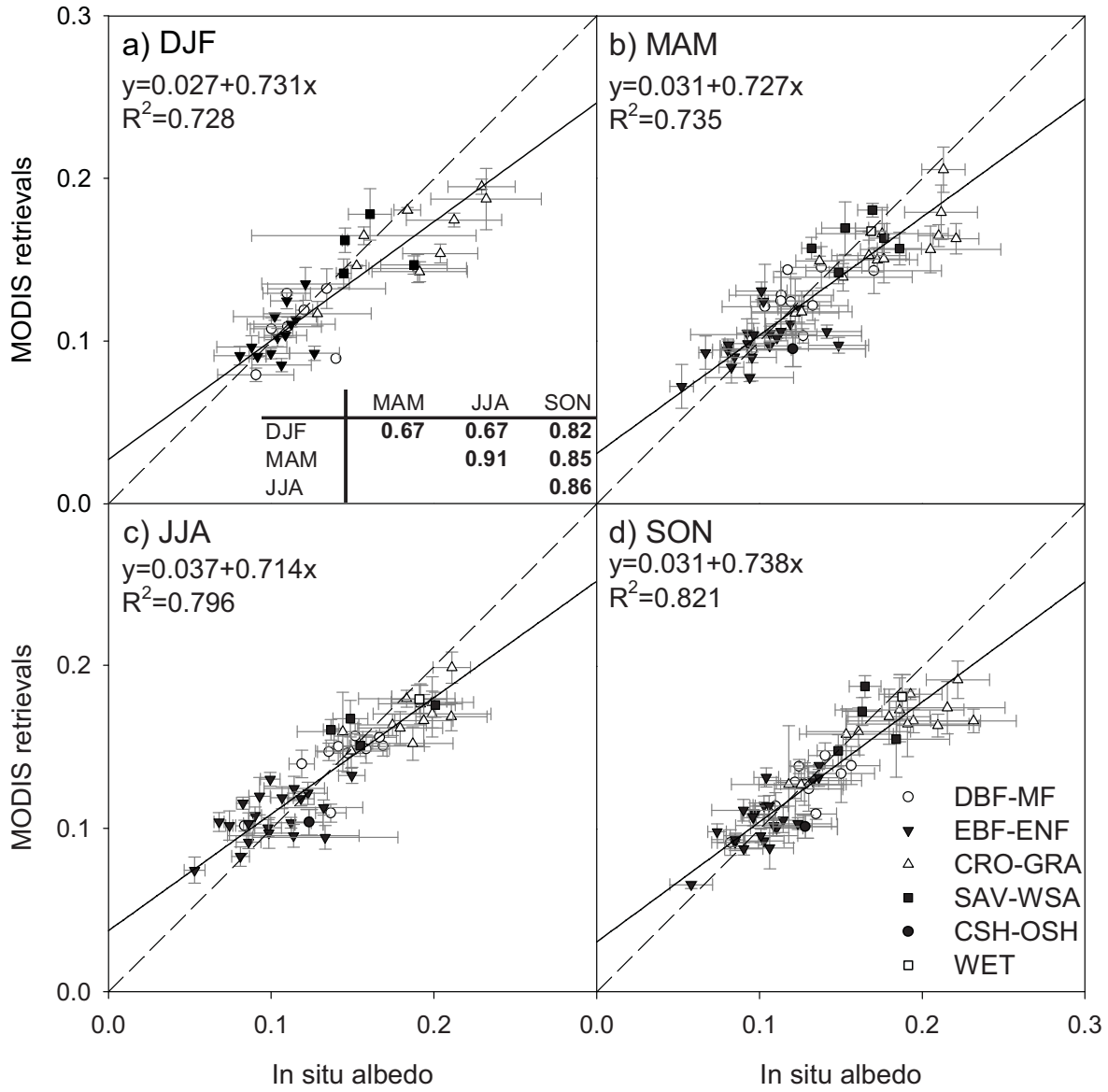


Figure 10

